

Discrimination of a medial functional module within the temporal lobe using an effective connectivity model: A CCEP study



Julien Krieg ^{a,b,*}, Laurent Koessler ^{a,b,c}, Jacques Jonas ^{a,b,c,f}, Sophie Colnat-Coulbois ^{d,e}, Jean-Pierre Vignal ^{a,b,c}, Christian G. Bénar ^{g,h,1}, Louis G. Maillard ^{a,b,c,e,1}

^a Université de Lorraine, CRAN, UMR 7039, Campus Sciences, Boulevard des Aiguillettes, 54500 Vandœuvre-lès-Nancy, France

^b CNRS, CRAN, UMR 7039, Campus Sciences, Boulevard des Aiguillettes, 54500 Vandœuvre-lès-Nancy, France

^c Service de Neurologie, Centre Hospitalier Universitaire de Nancy, 29 Avenue Du Maréchal de Lattre de Tassigny, 54000 Nancy, France

^d Service de Neurochirurgie, Centre Hospitalier Universitaire de Nancy, 29 Avenue Du Maréchal de Lattre de Tassigny, 54000 Nancy, France

^e Faculté de Médecine de Nancy, Université de Lorraine, 9 Avenue de La Forêt de Haye, 54500 Vandœuvre-lès-Nancy, France

^f Université Catholique de Louvain, 10 Place Du Cardinal Mercier, 1348 Louvain-La-Neuve, Belgium

^g Aix Marseille Université, Institut de Neurosciences des Systèmes, Marseille, F-13005 France

^h INSERM, UMR 1106, Marseille, 13005 France

ARTICLE INFO

Keywords:

Temporal lobe

CCEPs

Effective connectivity

Functional module

ABSTRACT

The temporal lobe is classically divided in two functional systems: the ventral visual pathway and the medial temporal memory system. However, their functional separation has been challenged by studies suggesting that the medial temporal lobe could be best understood as an extension of the hierarchically organized ventral visual pathway. Our purpose was to investigate (i) whether cerebral regions within the temporal lobe could be grouped into distinct functional assemblies, and (ii) which regions were central within these functional assemblies. We studied low intensity and low frequency electrical stimulations (0.5 mA, 1 Hz, 4 ms) performed during sixteen pre-surgical intracerebral EEG investigations in patients with medically intractable temporal or temporo-occipital lobe epilepsies. Eleven regions of interest were delineated per anatomical landmarks such as gyri and sulci. Effective connectivity based on electrophysiological feature (amplitude) of cortico-cortical evoked potentials (CCEPs) was evaluated and subjected to graph metrics. The amplitudes discriminated one medial module where the hippocampus could act as a signal amplifier. Mean amplitudes of CCEPs in regions of the temporal lobe showed a generalized Pareto distribution of probability suggesting neural synchronies to be self-organized critically. Our description of effective interactions within the temporal lobe provides a regional electrophysiological model of effective connectivity which is discussed in the context of the current hypothesis of pattern completion.

1. Introduction

Brain connectivity studies aim at characterizing specific integration pathways, whose complexity is at the origin of cognition. They rely on the assumption that high-level brain functions cannot be understood solely as the property of individual regions but instead result from interactions between distributed and functionally connected cortical areas (Zeki and Shipp, 1988; DeYoe et al., 1994; Keller et al., 2011), as shown for instance in occipito-temporal regions during face perception (Bentin

et al., 1996; Rossion et al., 2003; Barbeau et al., 2008). Studies of these networks have greatly benefited from the recent improvement in non-invasive imaging techniques such as Diffusion Tensor Imaging (DTI, Catani and Thiebaut de Shotten, 2008; Jones, 2008) or functional Magnetic Resonance Imaging (fMRI, Keller et al., 2013), as well as from the application of graph theory measures on resulting structural or functional connectivity matrices (Bullmore and Sporns, 2009; He and Evans, 2010; Wang et al., 2011).

In addition to neuroimaging techniques, numerous studies have used

* Corresponding author. Université de Lorraine, CRAN, UMR 7039, Campus Sciences, Boulevard des Aiguillettes, 54500 Vandœuvre-lès-Nancy, France.

E-mail address: julien.krieg@univ-lorraine.fr (J. Krieg).

¹ Equally contributed.

cortico-cortical evoked potentials (CCEPs) derived from low-frequency intra-cranial electrical stimulation in order to estimate ‘anatomical functional’ connectivity (reviewed in David et al., 2010). CCEPs allow studying the directionality and reciprocity of functional connections through the use of comparable bi-directional stimulations in pairs of ROIs (Buser and Bancaud, 1983; Wilson et al., 1990; Matsumoto et al., 2004, 2007; David et al., 2013; Keller et al., 2014a, 2014b; Entz et al., 2014; Enatsu et al., 2015). This paradigm is compatible with the concept of effective connectivity which evaluates the influence one neural population exerts on another (Friston, 1994).

Occurrence and amplitude of evoked potentials have been classically extracted from CCEPs. The CCEP occurrence has been calculated as the percentage of activated electrode sites per region (Catenoix et al., 2011; Almashaikhi et al., 2014a, 2014b), or as the percentage of responsive regions of interest across subjects (David et al., 2013). Matsumoto et al. (2004) suggested that this measure could provide functional and structural indices of connectivity between cortical regions, based on the observation of asymmetrical reciprocal connections between Wernicke's and Broca's areas.

The amplitude of the first peak of the CCEP, which reflects the degree of neural synchronization around the responsive electrode site, could represent an electrophysiological marker of the effective connectivity (Friston, 1994) between the stimulated and the remote activated areas. Matsumoto et al. (2007) extracted this parameter to build a precise functional connectivity map based on the assumption that the region with the highest amplitude of the CCEP field is the most strongly modulated by the stimulation site. These authors described a cortico-cortical functional network connecting somatotopically homologous medial and lateral motor cortical areas in a reciprocal manner.

Based on primate lesion or human neuropsychological, neuroimaging and electrophysiological studies, the temporal lobe has been functionally divided in two systems: the medial temporal system including hippocampus, amygdala, rhinal and parahippocampal cortices dedicated to declarative memory (Squire and Zola-Morgan, 1991; Eichenbaum and Cohen, 2001) and the ventral visual pathway including lateral and ventral occipito-temporal areas dedicated to object perception and categorization (Mishkin and Ungerleider, 1982; Tanaka, 1996; Grill-Spector, 2003; Kravitz et al., 2013). This concept includes also the fact that high-order sensory information from the ventral visual pathway and from other association areas (including the dorsal visual pathway) project to the medial temporal lobe structures where they are associated to form memories (Suzuki, 2009).

However, the limits between the medial memory system and the ventral visual system and even the bi-modular organization of the temporal lobe have been challenged by several monkey and human lesions and neuroimaging studies. These studies have suggested a role of the perirhinal cortex in complex visual discrimination based on the conjunction of elementary features (see Buckley et al., 2001; Moss et al., 2005 for examples). It has been suggested that structures within the medial temporal lobe memory system could be best understood as an extension (Bussey and Saksida, 2007; Baxter, 2009; Cowell et al., 2010) of the hierarchically organized ventral visual pathway (Felleman and Van Essen, 1991). Warren et al. (2012) showed that lesions of medial temporal lobe structures could impair visual identification of novel items based on online representations, suggesting collaborative interactions between medial temporal structures and neocortices during these tasks.

Reciprocal modulation of perceptive structures by the medial temporal system has been discussed in cognition during reminiscence (Bancaud et al., 1994; Bartolomei et al., 2004; Barbeau et al., 2005), recency processes (Babiloni et al., 2004) or arousal (Liégeois-Chauvel et al., 2014). However, the reciprocal effective connectivity (Friston, 1994) from the medial temporal system on the ventro-lateral temporal

Table 1
List of acronyms.

Acronym	Meaning	Acronym	Meaning
SEEG	Stereo-Electro-EncephaloGraphy	STG	Superior Temporal Gyrus
CCEP	Cortico-Cortical Evoked Potential	O1	Peak of first significant component of the CCEP
CT-scan	Computerized Tomography Scanner	EM	Exploration Matrix (with e_{ij} elements)
f/MRI	Functional/anatomical Magnetic Resonance Imaging	OM	Occurrence Matrix (with o_{ij} elements)
S1 to S16	Subject 1 to Subject 16	AM	Amplitude Matrix (with a_{ij} elements)
S1bis	Second SEEG exploration of S1	SEAM	Standard Error on Amplitude through subjects Matrix (with s_{ij} elements)
DNE	Dysembryoplastic NeuroEpithelial tumour	σ_{ij}	Standard deviation of amplitudes through subjects (ROI _i towards ROI _j)
ROI TP	Region of Interest Temporal Pole	R	Correlation Coefficient
		STD-TW	Standard Deviation Through Weights (for the whole AM matrix)
Amyg	Amygdala	RSD	Relative Standard Deviation
aHipp	Anterior Hippocampus	SE-TW	Standard Error Through Weights (for one node or ROI)
pHipp	Posterior Hippocampus	GOF	Goodness Of Fit
aPHG	Anterior ParaHippocampal Gyrus (rhinal cortex)	R ²	Coefficient of Determination (square of the Correlation Coefficient)
pPHG	Posterior ParaHippocampal Gyrus	RMSE	Root Mean Square Error
aFG	Anterior temporal Fusiform Gyrus	Q	Coefficient of maximization (Newman's spectral modularity)
pFG	Posterior temporal Fusiform Gyrus	AM-M	Medial module in the modularity of AM
ITG	Inferior Temporal Gyrus	AM-VLP	Ventral lateral polar subnetwork in the modularity of AM
MTG	Middle Temporal Gyrus	SNR	Mean signal-to-noise ratio through snr_{ij} elements

neocortex has been scarcely described in human. A human study based on occurrence of CCEPs focused on hippocampal efferences and showed effective projections to various ventro-lateral temporal neocortices with highest occurrence rates at the temporal pole and the anterior fusiform gyrus (Catenoix et al., 2011).

Based on the hypothesis that electrophysiological features could contribute to assess a functional segregation within the temporal lobe and to characterize central cerebral regions, we used intra-cerebral CCEPs performed during stereo-electroencephalography in humans to investigate (i) whether cerebral regions within the temporal lobe could be grouped in distinct functional assemblies (namely the ventral visual pathway and the medial temporal system) based on their properties of effective connectivity, and (ii) which regions of interest were central within these functional assemblies. For this purpose, we used graph metrics applied on amplitudes of CCEPs to describe and compare, in a model of effective connectivity, the indices of centrality and functional segregation within the human temporal lobe.

2. Methods

2.1. Subjects

We analyzed recordings from 16 stereo-electroencephalography (SEEG, see Table 1 for a list of acronyms) explorations in 15 epileptic patients (Subject 1 underwent two SEEG explorations, see Table 2 in

annex for patients' characteristics) with drug-resistant structural focal epilepsy involving temporal or occipital temporal regions. SEEG recordings were performed in order to delineate the epileptogenic zone (Bancaud and Talairach, 1973). The patients were recorded 24 h a day for four to seven days in the epilepsy unit of the University Hospital of Nancy. Intracerebral electrical stimulation sessions were applied from the second to the fourth day for epileptogenic zone delineation and functional mapping (Rutecki et al., 1989; Chauvel et al., 1993; Valentín et al., 2002; David et al., 2008). A session of resting state (5 min) was recorded, immediately before sessions of electrical stimulations. During the stimulation and resting state sessions, the patients were reclined in their bed in a relaxed state. They were kept awake, eyes open. Each patient gave written informed consent for their participation to this study which was approved by the ethic committee of the University Hospital of Nancy.

2.2. SEEG placement and recordings

The electrode implantation sites were chosen according to non-invasive data collected during the earlier phase of investigation in order to localize and delineate the zone of epileptic seizure onset and early propagation (Jonas et al., 2014). Stereotactic placement of intracerebral electrodes (Dixi Medical, Besançon, France), consisting of 5–18 contiguous contacts of 2-mm long separated by 1.5 mm, was performed as follows: after induction of general anesthesia, the Leksell G-frame (Elekta S.A., Stockholm, Sweden) was positioned on the patient's head and a stereotactic MRI (3D SPGR T1 weighted-sequence, TR: 20 ms, TE: 6 ms matrix 512*512, with double injection of gadolinium, Signa 1.5 T; General Electric Medical System, Milwaukee, United States) was carried out. MRI was imported into a computer-assisted stereotactic module (Leksell Surgiplan; Elekta S.A., Stockholm, Sweden), and electrode trajectories were calculated according to pre-operative planning, with careful avoidance of vascular structures. A post-operative stereotactic CT-scan was then applied and fused with pre-operative MRI to determine the precise anatomical

gyral and sulcal position of each contact. The signal was recorded at a 512 Hz sampling rate on a 128-channels amplifier (two SD-LTM 64 Headbox; Micromed, Italy). The acquisition filter was an analog 0.18 Hz high-pass filter. The reference was a prefrontal-central scalp electrode (FPz).

2.3. Intracerebral electrical stimulations

Standard cortical bipolar electrical stimulations were used for functional mapping in all subjects as part of pre-surgical evaluation and applied on pairs of adjacent contacts. Previous studies observed that variation of the electrical intensity of the stimulation impacts the amplitude and latency of the first component (usually called 'N1' component, Matsumoto et al., 2004) of the CCEP (Rutecki et al., 1989; Wilson et al., 1990). Lower intensity stimulation leads to lower amplitude and longer latency of the 'N1' component. We applied stimulations with equal intensity in order to extract comparable patterns through structures and patients. The intracerebral stimulations were performed at 1 Hz during 60 s (60 pulses) at an intensity of 0.5 mA with bi-phasic square wave electric currents, a pulse width of 2 ms per phase. The delivered charge density was equal to 20 $\mu\text{C}/\text{cm}^2/\text{phase}$, which corresponds to the mean range of the charge density used by Wilson et al. (1990) who investigated the medial temporal lobe with similar electrodes. We observed that hippocampal stimulation of adjacent pairs of contacts could show sensible different patterns and spatial distribution of CCEPs in the temporal lobe at the contact level. We thus heuristically estimated the diameter of the volume of the delivered effective charge density as inferior or equal to the length of stimulated contact plus the distance between adjacent contacts (5 mm). Contacts to be stimulated were chosen the first day of implantation by the neurologists (J.J., L.G.M.), according to their anatomical location on the CT-scan/MRI reconstructions (BrainLab AG, Germany) in grey matter. According to the spatial resolution of MRI (about 1 mm) and the diameter of the volume of the charge density delivered (about 5 mm), we estimated the error on spatial

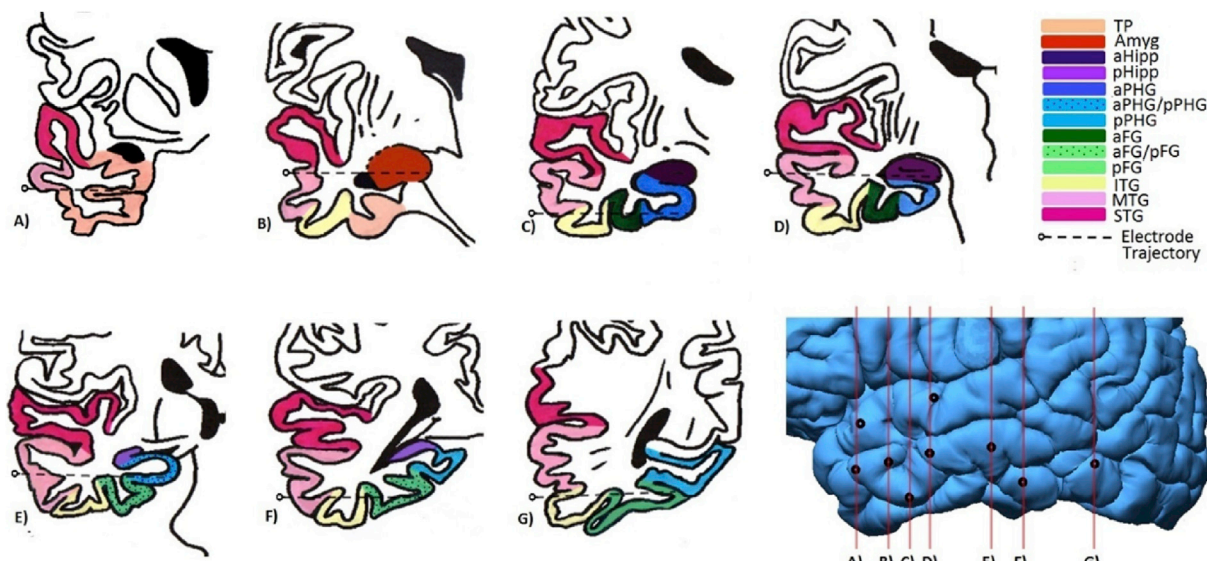


Fig. 1. Example of morphological delineation in regions of interest of the right temporal lobe of Subject 13 where all right ROIs have been explored but pHipp. From left to right, from top to bottom, anatomical illustration of antero-posterior slice taken from the CT-scan/MRI reconstruction (BrainLab AG, Germany) at 7 of the 9 electrode locations in the right hemisphere. The electrode trace is schematized by dotted lines. Each slice is relative to one vertical red line on the sagittal view of the 3D-volume extraction at the right bottom. Electrodes entry points were represented by black dots. Electrodes entering the superior temporal gyrus are almost in the same plane as A) and D). The volume extraction was performed with Brainstorm 3.1 (Tadel et al., 2011), which is documented and freely available for download online under the GNU general public license (<http://neuroimage.usc.edu/brainstorm>). See Table 1 for a list of acronyms.

cortical structure mapping to be around ± 3 mm. Evoked potentials on contacts directly adjacent to couples of stimulated contacts and/or on contacts belonging to the stimulated ROI were not taken into consideration. A total of 424 contacts were stimulated and 862 were recorded through the 16 SEEG explorations (see Table 3 in annex for details on recorded and stimulated structures).

2.4. Region of interest (ROI)

For each subject, we (J.J., L.G.M.) visually delineated within the temporal lobe 11 sub-lober Regions Of Interest (ROI, Fig. 1) for each hemisphere, based on anatomical landmarks (Duvernoy et al., 1992; Destrieux et al., 2010; Huntgeburth and Petrides, 2012) observed on the CT-scan/MRI reconstruction (BrainLab AG, Germany). The temporal lobe was divided into: temporal pole (TP), amygdala (Amyg), anterior hippocampus (aHipp), posterior hippocampus (pHipp), anterior parahippocampal gyrus (aPHG, rhinal cortex), posterior parahippocampal gyrus (pPHG), anterior temporal fusiform gyrus (aFG), posterior temporal fusiform gyrus (pFG), inferior temporal gyrus (ITG), middle temporal gyrus (MTG) and superior temporal gyrus (STG). According to Wilson et al. (1990), who showed different patterns of connectivity along the hippocampus, we divided anterior and posterior hippocampus at its midline, visually determined on the CT-scan/MRI sagittal plan (J.J., L.G.M.). aPHG was delineated anteriorly by the uncus and posteriorly by the end of the rhinal sulcus. pPHG was delineated anteriorly by aPHG, and posteriorly by the lingual gyrus. aFG and pFG were delineated medially by rhinal and collateral sulci respectively and laterally by the lateral occipito-temporal sulcus. The temporal pole was delineated medially by the uncus, and laterally by the termination of both the anterior superior and inferior temporal sulci. Consequently, lateral temporal ROIs ITG and MTG were delineated anteriorly respectively according the end of the inferior temporal and superior temporal sulci.

Posteriorly, ITG and MTG were delineated in the sagittal plan respectively by the temporo-occipital incisure and the anterior occipital sulcus. STG was delineated anteriorly by the end of the superior temporal sulcus, posteriorly by the inferior part of the angular gyrus, medially by the insula at the bottom of the sylvian fissure. Depth of sulcus was the morphological limit between ROIs. Ambiguous contacts, located at the depth of sulcus were attributed to the most medial ROI. We analyzed both hemispheres in an ipsilateral and regional effective connectivity model.

2.5. Data processing

Effective connectivity was first evaluated by detecting cortico-cortical evoked potentials to define their occurrence (Wilson et al., 1990; Matsumoto et al., 2004, 2007; Catenoix et al., 2011; Almashaikh et al., 2014a, 2014b; Keller et al., 2014a; Entz et al., 2014). We primarily detected the electrical pulse artifact on monopolar recordings with an amplitude threshold of 2000 μ V. We segmented the signal from -0.5 to 0.5 s relative to the onset of the pulse defined as time zero. Then, a bipolar montage of adjacent contacts within each electrode was applied. Data was filtered with an Infinite Impulse Response (IIR, transition bandwidth 0.2 Hz, order 6) high-pass filter with 0.5 Hz cut off frequency which uses reverse filtering to prevent phase distortion of the signal. Mean CCEP peaks detection was performed by first selecting time points whose absolute value was higher than two preceding and two succeeding time points. Then, the validity of detected peaks, in terms of energy, was controlled with the presence of a simultaneous peak in the root mean square of the CCEP computed across trials (Enatsu et al., 2015). The statistical significance of each detected peak was finally assessed by a *t*-test with multiple comparison correction (as described in next subsection). All these preprocessing steps were automatized.

We simulated the processing chain of the acquisition system

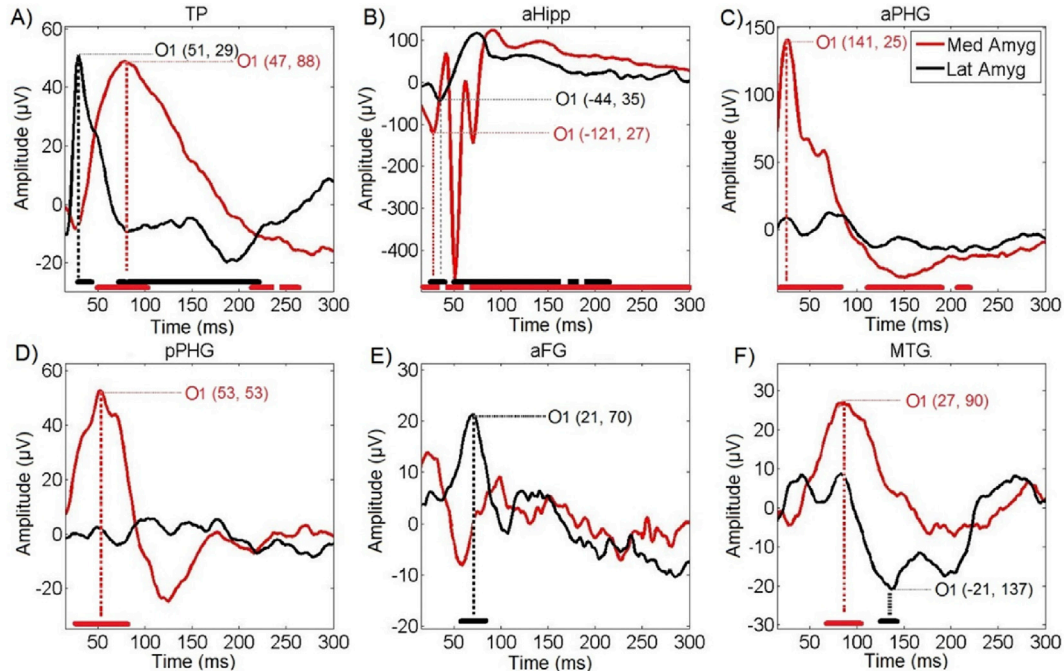


Fig. 2. Examples of detections of O1 peaks of CCEPs at same bipolar pair of contacts in different ROIs from two stimulation runs at medial (red) and lateral (black) bipolar pairs of contacts located within the amygdala of Subject 13. Centers of stimulation dipoles were separated by 7 mm. Significant temporal clusters were reported at the bottom for each curve. Amplitude (vertical axe) and latency (horizontal axe) of detected O1 peaks are shown into brackets. A) Temporal Pole (TP) -B) anterior Hippocampus (aHipp) -C) anterior Parahippocampal Gyrus (aPHG) -D) posterior Parahippocampal Gyrus (pPHG) -E) anterior Fusiform Gyrus (aFG) -F) Middle Temporal Gyrus (MTG).

(System Plus Evolution, Micromed, Italy) via Simulink (Matlab R2011a, The Mathworks) in order to quantify the delay of spurious signal stemming from the stimulation artifact on each recording. We estimated probable residuals of the electrical stimulation artifact with an amplitude superior to 10 μ V through trials until 14 ms post-stimulation onset. Therefore, we choose our interval of interest from 15 to 300 ms post-stimulation in latency, and from 10 μ V to 2000 μ V in amplitude. Because peaks of evoked potentials in the temporal lobe, especially in medial temporal structures usually occur 300 ms after

cognitive stimulation such as the P300 component (Halgren et al., 1995, 1998; Rey et al., 2014), or that CCEPs in lateral temporal lobe from the stimulation of the hippocampus could happen until 300 ms (Catenoix et al., 2011), we choose a large time interval to allow possible peak detection in late downstream targets. We focused on the earliest significant peak of the mean CCEP through trials for each contact (Matsumoto et al., 2004). In this study, due to the complexity of observed CCEP dynamics in medial structures (Rutecki et al., 1989), their possible late occurrence (Catenoix et al., 2005, 2011; Rey et al.,

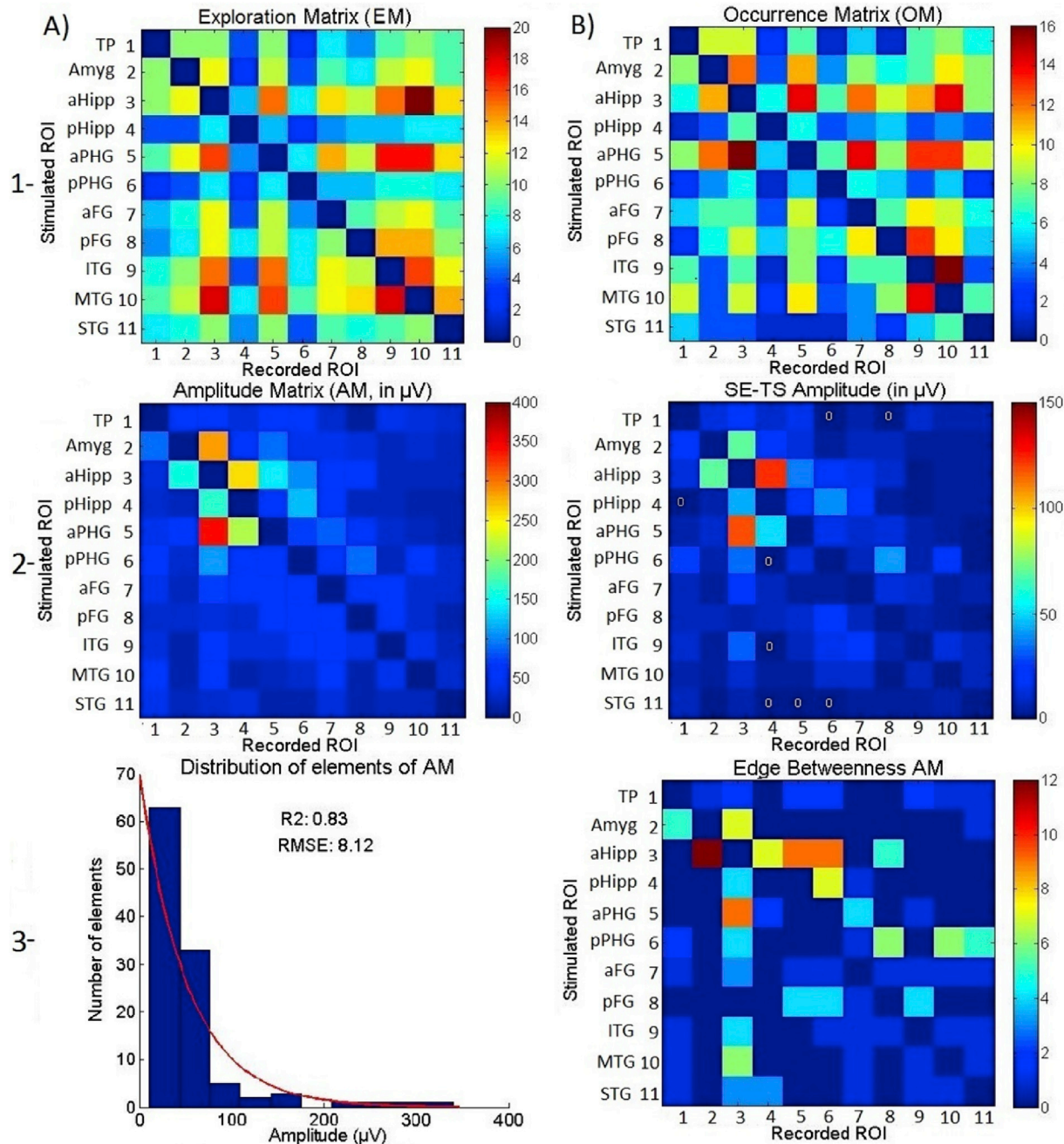


Fig. 3. 1-A) Exploration Matrix (EM), number of ipsilateral SEEG explorations through subjects and hemispheres per edge. 1-B) Occurrence Matrix (OM), number of ipsilateral responsive links per edge. 2-A) Amplitude Matrix (AM), color code [0; 400 μ V]. 2-B) Standard Error on Amplitude through subjects Matrix (SEAM) color code [0, 150 μ V]. Edges with null s_{ij} value (single occurrence) are marked with white '0'. 3-A) Probability distribution of edges values of AM. Elements of AM showed a generalized Pareto distribution. 3-B) Edge betweenness (Number of shortest paths from all nodes passing through each edge) for AM, color code [0; 12]. Recorded and stimulated ROIs are reported on horizontal and vertical axes respectively on each matrix.

2014) and because the polarity of the first evoked component could vary in SEEG, we labeled this first detected peak of CCEP as ‘O1’ (derived from ‘first occurrence’). It avoids confusion with the first evoked component (‘A1’ or ‘N1’) occurring in the 10–50 ms time interval defined in previous studies (Keller et al., 2014a; Entz et al., 2014). Large time interval is adapted to the time scale of effective interactions between neocortical and medial structures (Rey et al., 2014). The amplitude of this first peak ‘O1’ reflected the strength of information transfer regardless of the possible direct or indirect character of the underlying pathway (Fig. 2). We rejected segments with epileptic activity after expert visual analysis of the trials (L.G.M., J.P.V.). Each stimulation dataset resulted in 13–60 trials. The same methodology was applied for the baseline activity taking 100 consecutive seconds of resting state for each subject. We visually selected 60 trials of 1 s each with baseline activity devoid of artifact. All electrophysiological signals have been processed using Matlab (R2011a, the MathWorks) and EEGLAB 9 (Delorme and Makeig, 2004).

2.6. Statistical analysis of the occurrence of the CCEP

For each contact of each subject, we compared with a classical parametric *t*-test the evoked activity generated in the interval of interest from the dataset of stimulation to the background activity recorded during the resting state period (threshold alpha-value = 0.01). For each subject, the same dataset of rest was used as baseline for all stimulation sites. In order to take into account the multiple comparison within each ROI, a permutation test based on the temporal cluster measure was performed (Maris and Oostenveld, 2007). The cluster measure consisted in the sum of consecutive *t*-values above a given threshold (alpha-value = 0.01): this measure is sensitive to both small significant intervals with high *t*-values and long intervals with small *t*-values. Trials of each contact for each stimulation run were randomly permuted 100 times with the same number of trials extracted from the baseline dataset. Permutated sets were compared with the cluster measure. The maximum cluster value at each contact was selected at each permutation. We then chose the maximum cluster across the 100 permutations for each contact, which is equivalent to a Monte Carlo procedure at *p*-value = 0.01. A spatial correction was added by selecting the maximum cluster value across contacts within each ROI. Finally, cluster values in the original dataset superior or equal to the maximum cluster value extracted from permutations were kept and the others were removed through all contacts within each ROI. The O1 potential was defined as the earliest CCEP peak lying in a significant cluster in the original dataset for each contact (Fig. 2). Amplitude feature of the peak of the O1 potential was then extracted for further processing.

2.7. Calculation of CCEP patterns

Once significant activity was detected, the occurrence and absolute value of the amplitude of the O1 peak were reported according to the ROI delineation for each subject. Knowing that low connectivity between both temporal lobes was observed in previous studies (Buser et al., 1971; Wilson et al., 1990, 1991; Lacruz et al., 2007), we focused on ipsilateral CCEPs. In bilateral explorations, similar couples of ROI were analyzed in the same ipsilateral framework as two distinct explorations. We reported in the Exploration Matrix (EM, with elements e_{ij} , ROI ‘*i*’ towards ROI ‘*j*’, eq. (1) and Fig. 3-1-A), as the sum of all explorations of each couple of ROIs, how many times one couple of ROIs were stimulated and recorded through hemispheres explored (15 left and 10 right hemispheres, see Table 3 in annex for details on recorded and stimulated structures).

$$e_{ij} = \begin{cases} \sum_{k=1}^{N_H} (\text{expl}_k) & \text{if } i \neq j, \\ 0 & \text{if } i = j. \end{cases} \quad \text{with } i \text{ and } j \in [1, 11] \quad (1)$$

With expl_k equal to 1 if ROI_{*j*} through stimulations of ROI_{*i*} was recorded for each hemisphere, 0 otherwise. $k \in [1, N_H]$, $N_H=25$ is the total number of hemispheres explored through subjects.

For each hemispheric exploration, we computed the occurrence measure by testing whether at least one other contact in another ROI showed a CCEP through stimulations. If this was the case, the directed link between ROIs was set to 1 for this stimulation (‘responsive’ link), 0 otherwise. The final Occurrence Matrix (OM with elements o_{ij} , eq. (2) and Fig. 3-1-B) was computed as the sum across explorations of the directed link values (0 or 1) for each ROI. In order to increase the robustness of observations at least three different patients, independently of the number of hemispheres explored in each subject, was used to compute each element o_{ij} .

$$o_{ij} = \begin{cases} \sum_{k=1}^{e_{ij}} (\text{peakocc}_k) & \text{if } i \neq j, \\ 0 & \text{if } i = j. \end{cases} \quad \text{with } i \text{ and } j \in [1, 11] \quad (2)$$

With peakocc_k equal to 1 if the link is ‘responsive’ in ROI_{*j*} through stimulations of ROI_{*i*}, 0 otherwise. $k \in [1, e_{ij}]$, e_{ij} is defined by (eq. (1)).

For each subject and each responsive link in one hemisphere, absolute values of the amplitude from all O1 peaks were averaged through contacts and stimulations. We then computed the grand average of the averaged peak amplitude across all responsive links to construct the Amplitude Matrix (AM with elements a_{ij} , eq. (3) and Fig. 3-2-A).

$$a_{ij} = \begin{cases} 1/o_{ij} \sum_{l=1}^{o_{ij}} x_l & \text{if } i \neq j, \\ 0 & \text{if } i = j. \end{cases} \quad \text{with } i \text{ and } j \in [1, 11] \quad (3)$$

$$\text{and } x_l = 1/N(S_l)_{\text{RCS}} \sum_{m=1}^{N(S_l)_{\text{RCS}}} |\text{peakampl}_m|$$

With peakampl_m equal to the amplitude of the detected O1 peak (‘responsive’ link) on each responsive contact in ROI_{*j*} through stimulations of ROI_{*i*}, $m \in [1, N(S_l)_{\text{RCS}}]$. For each subject S_l with responsive link ROI_{*i*} towards ROI_{*j*}, $N(S_l)_{\text{RCS}}$ is the number of responsive contacts in ROI_{*j*} through stimulations of ROI_{*i*}. $N(S_l)_{\text{RCS}}$ could vary between 1 to the number of recorded contacts in ROI_{*j*} multiplied by the number of stimulations of ROI_{*i*} for each subject (Table 3, annex). x_l is equal to the mean amplitude of all detected O1 peaks across contacts in ROI_{*j*} through stimulations of ROI_{*i*} in a single exploration. $l \in [1, o_{ij}]$, o_{ij} is defined by (eq. (2)).

We also constructed the Standard Error on Amplitude through subjects Matrix (SEAM, with elements s_{ij} , eq. (4) and Fig. 3-2-B) across responsive links.

$$s_{ij} = \begin{cases} \frac{\sigma_{ij}}{\sqrt{o_{ij}}} & \text{if } i \neq j \text{ and } \forall o_{ij} > 1, \\ 0 & \text{if } i = j \text{ or } o_{ij} = 1. \end{cases} \quad \text{with } i \text{ and } j \in [1, 11] \quad (4)$$

Table 4

Coefficient of correlation (R) between elements of matrices of the constructed model ($\forall o_{ij} > 1$; 102 elements per matrix).

R	EM	OM	AM	SEAM
EM	1	0.78	-0.002	-0.03
OM	0.78	1	0.29	0.2
AM	-0.002	0.29	1	0.93
SEAM	-0.03	0.2	0.93	1

and $\sigma_{ij} = \sqrt{1/(o_{ij}-1) \sum_{l=1}^{o_{ij}} (x_l - a_{ij})^2}$ $\forall o_{ij} > 1$. σ_{ij} is equal to the standard deviation of x_l values through responsive links for a couple of stimulated/recoded ROIs. x_l and a_{ij} are defined in (eq. (3)). $l \in [1, o_{ij}]$, o_{ij} is defined by (eq. (2)).

We calculated the mean signal-to-noise ratio on averaged amplitude estimation through edges \overline{SNR} by first calculating the signal-to-noise ratio for each edge snr_{ij} (eq. (5)), such as:

$$snr_{ij} = \begin{cases} \frac{a_{ij}}{\sigma_{ij}} & \text{if } i \neq j \text{ and } \forall o_{ij} > 1, \\ 0 & \text{if } i = j \text{ or } o_{ij} = 1. \end{cases} \quad \text{with } i \text{ and } j \in [1, 11] \quad (5)$$

\overline{SNR} was defined as the mean through non-null snr_{ij} values estimated for each edge ($\forall o_{ij} > 1$; 102 values). a_{ij} and o_{ij} are defined by (eq. (3)) and (eq. (2)) respectively. σ_{ij} is defined in (eq. (4)).

We constructed the effective connectivity matrix by considering each ROI ($n = 11$) as a network node. Bi-directional stimulations of couple of ROIs in the whole temporal lobe allowed us to draw a directed and weighted connectivity matrix from amplitudes (AM, with elements a_{ij} , Fig. 3-2-A). Amplitude elements were considered as weights with the hypothesis that the higher the induced amplitude of the CCEP, the stronger the connectivity weight between a pair of nodes. Probability distribution of elements of AM has been fitted with the ‘dfittool’ function of Matlab (R2011a, The Mathworks). In order to evaluate possible linear correlation between variables of the model, we calculated the correlation coefficient (R) between elements of constructed matrices ($\forall o_{ij} > 1$; Table 4).

2.8. Graph theoretical analysis

To evaluate the effective organization of the network we used graph metrics as described in Rubinov and Sporns (2010). These measures allow determining the functional role of nodes (ROIs) or edges (links between ROIs) within connectivity matrices. All graph metrics have been computed using the Matlab Brain Connectivity Toolbox (<http://www.brain-connectivity-toolbox.net>) accompanying the previously cited article. We used generalized measures for weighted and directed networks. A brief recall of the definitions is presented in the following.

2.8.1. Centrality of nodes and edges

We characterized individual node according to its centrality within the temporal lobe. In particular, we used the node strength and betweenness centrality. These measures are directly related to the functional impact of one node on the network. This impact in information transfer could rely on the number of strong connections or how much one node improves the accessibility of other nodes in the whole network. The node strength is defined as the sum of its weights. Because our network is

directed, we may also distinguish the strength of *inward* ('in') and *outward* ('out') links (Rubinov and Sporns, 2010). We also calculated the ratio 'in/out' strength in order to detect asymmetries between *inward* and *outward* links for each node (Entz et al., 2014).

Betweenness centrality is defined as the fraction of all shortest paths in the network that passes through a given node. The shortest path between two nodes is the sequence of edges whose sum of the inverse of weights is minimum. Nodes connecting fragmented parts of the network have high betweenness centrality. We also analyzed the extension of that measure to the edge values as the *edge betweenness* (Rubinov and Sporns, 2010).

2.8.2. Functional segregation of nodes: Newman's spectral modularity

Newman's spectral modularity measure is based on a subdivision of the network into groups of nodes (modules), with maximal within-group strengths, and minimal between-groups strengths (Girvan and Newman, 2002). We used an optimization algorithm developed by Newman (2006) that is adequate for small networks (Rubinov and Sporns, 2011). This measure results in a coefficient of maximization Q, which is statistically high compared to randomly permuted networks if a functional segregation is likely to underlie the original network, and low otherwise. In order to distinguish true modules in the segregation, we compared the *mean within-* and *between-module strengths*. Statistics are described in the following paragraph “Statistical analysis of graph metrics”.

2.9. Statistical analysis of the graph metrics

We considered as significant the values of strengths which were out of one standard deviation both sided from the mean through ROI. While the interpretation of low values of betweenness was not relevant in this study, we considered only maximum values out of one standard deviation from the mean through ROI (Van den Heuvel and Sporns, 2011). Concerning Newman's spectral modularity, we used a randomization algorithm that generated 1000 permutations of weights at each node keeping equal the mean strength of nodes through permutations (Rubinov and Sporns, 2011). Then, the original network was considered as showing a significant spectral modularity if its coefficient of maximization Q_{origin} provided by the measure was higher than 95 per cent of the coefficients of maximization Q_{perm} stemming from the permuted networks. The mean within- and between-modules strengths were compared with Mann-Whitney-Wilcoxon rank sum statistics.

3. Results

3.1. Construction of the effective connectivity matrix AM

We extracted the averaged amplitude of the detected O1 peak of CCEPs. We drew a directed and weighted connectivity matrix using this

Table 5

Summary of measures of centrality and functional segregation applied on the effective connectivity matrix AM. The red and blue font colors are indexing nodes with coefficients out of one standard deviation both sided from the mean of coefficients through nodes (high or low respectively). In Newman's spectral modularity “M” and “VLP” refer to the module AM-M and the subnetwork AM-VLP. Green font color is indexing the significant module.

AM	Graph Metrics	TP	Amyg	aHipp	pHipp	aPHG	pPHG	aFG	pFG	ITG	MTG	STG
Centrality of nodes	Strength 'total'	822	1117	2071	1315	1506	1154	941	754	706	612	467
	'out'	376	701	865	532	928	555	442	377	391	317	248
	'in'	446	416	1206	783	578	599	499	377	315	295	219
	'in/out'	1.19	0.59	1.39	1.47	0.62	1.08	1.13	1	0.81	0.93	0.88
	Betweenness	1	3	32	2	6	14	0	3	0	0	0
Functional segregation	Modularity	VLP	M	M	M	M	VLP	VLP	VLP	VLP	VLP	VLP

parameter (AM, mean = 52 μ V, STD-TW = 53 μ V, RSD = 1, Fig. 3-2-A). Elements of AM showed a generalized Pareto distribution (location: $\mu = 0$, scale: $\sigma = 52$, shape: $k = 0.003$, mean = 52 μ V, STD-TW = 52 μ V, RSD = 1; GOF: R2 = 0.83, RMSE = 8.12; Fig. 3-3-A)). Less than ten per cent of edge values of AM were extracted from single occurrence ($o_{ij} = 1$; $s_{ij} = 0$; Fig. 3-1-B and 2-B). Four edges involving the hippocampus showed very high mean amplitudes (superior than 200 μ V, Fig. 3-2-A): aPHG- > aHipp ($340 \pm 118 \mu$ V), Amyg- > aHipp ($283 \pm 69 \mu$ V), aHipp- > pHipp ($260 \pm 123 \mu$ V), aPHG- > pHipp ($219 \pm 52 \mu$ V). Six edges involving the hippocampus showed high mean amplitudes (between 100 and 200 μ V, Fig. 3-2-A): pHipp- > aHipp ($168 \pm 43 \mu$ V), aHipp- > Amyg ($161 \pm 69 \mu$ V), aHipp- > aPHG ($143 \pm 35 \mu$ V), pHipp- > pHipp ($123 \pm 38 \mu$ V), pHG- > aHipp ($110 \pm 34 \mu$ V), aHipp- > pHG ($103 \pm 17 \mu$ V). All these ten edges with amplitude superior than 100 μ V (9.1% of the total number of edges) accounted for 33.3% of the sum of all amplitude edges in the temporal lobe.

We calculated the correlation coefficient (R) between elements of each matrix constructed ($\forall o_{ij} > 1$; Table 4). Results showed a strong correlation between EM and OM matrices ($R = 0.78$), because the more a couple of ROI was explored, the more the number of occurrences were likely to be high. Results also showed a strong correlation between AM and SEAM matrices ($R = 0.93$) such that the higher the amplitudes, the higher the standard error on amplitudes through subjects. All other correlation coefficients were inferior to 0.3, such that no linear relationship between the number of explorations or occurrences and the amplitudes or the standard error on amplitudes were found. The estimated mean signal-to-noise ratio on amplitudes through edges \overline{SNR} was equal to 3.1, meaning amplitude weights were on average around three times higher than the inter-subject amplitude variability.

3.2. Results on graph metrics applied on the effective connectivity matrix AM

The following section synthesizes the results that are detailed in Table 5 (indices of centrality and modularity) and in Fig. 3 (AM, SEAM and edge betweenness). Amplitudes and the relative standard error through subjects are shown into brackets for all described edges of ROI_j towards ROI_i ($a_{ij} + - s_{ij} \mu$ V).

3.2.1. Centrality of different ROIs in the temporal lobe

3.2.1.1. Centrality of the amygdala (Amyg). All averaged amplitude of CCEPs inwards of the amygdala were lower than their reciprocal outwards (low ‘in/out’ strength). Among limbic structures, the amygdala was the ROI with the lowest averaged amplitude inwards. Within the temporal lobe, apart from aHipp ($161 \pm 69 \mu$ V), aPHG ($51 \pm 10 \mu$ V) and TP ($44 \pm 13 \mu$ V), no structure elicited O1 peak averaged amplitude above 40 μ V within the amygdala. The amygdala was also the second structure, after the rhinal cortex, to provoke very high averaged amplitude of CCEPs in the anterior hippocampus ($283 \pm 69 \mu$ V). These characteristics contributed to the low ‘in/out’ amplitude strength of the amygdala in the whole network.

3.2.1.2. Centrality of the anterior hippocampus (aHipp). aHipp was the most central node according to the results on AM (high ‘total’, ‘out’, ‘in’ and ‘in/out’ strengths). The highest aHipp potentials were evoked by the stimulation of aPHG and Amyg ($340 \pm 118 \mu$ V and $283 \pm 69 \mu$ V respectively). They were the highest averaged amplitudes recorded in the whole temporal lobe (high ‘in’ strength). In return, aHipp elicited the highest amplitude potentials of Amyg ($161 \pm 69 \mu$ V), pHipp ($260 \pm 123 \mu$ V) and aPHG ($143 \pm 35 \mu$ V) (high ‘out’ strength). Apart from pHipp and pFG, all averaged amplitude of CCEPs inwards of the anterior

hippocampus were higher than their reciprocal outwards (high ‘in/out’ strength). These characteristics contributed to significant high betweenness centrality (Table 5) meaning that aHipp was a central relay in the temporal lobe evoking the highest amplitude potentials in other limbic structures (‘edge betweenness’, Fig. 3-3-B). In summary, the anterior hippocampus showed amplified evoked potentials by the stimulation of amygdala and rhinal cortex and elicited amplified potentials in limbic structures.

3.2.1.3. Centrality of the posterior hippocampus (pHipp). Apart from pHG, aFG and MTG, all averaged amplitude of CCEPs inwards of the posterior hippocampus were higher than their reciprocal outwards (high ‘in/out’ strength). The highest pHipp mean potential ($260 \pm 123 \mu$ V) was evoked by the stimulation of aHipp while aHipp showed lower averaged amplitude ($168 \pm 43 \mu$ V) from the stimulation of pHipp. Also, pHipp strongly modulated pHG ($123 \pm 38 \mu$ V) while pHG slightly modulated pHipp (54μ V, single occurrence). In summary, pHipp showed amplified evoked potentials mainly provoked by anterior limbic structures and strongly modulated the posterior parahippocampal gyrus.

3.2.1.4. Centrality of the rhinal cortex (aPHG). The rhinal cortex was a central structure within the temporal lobe (high ‘total’, ‘out’ and low ‘in/out’ strengths). aPHG elicited the highest amplitude of the network in aHipp ($340 \pm 118 \mu$ V) which strongly impacted its ‘total’, ‘out’ and ‘in/out’ strengths. aHipp and Amyg elicited highest mean amplitudes of aPHG ($143 \pm 35 \mu$ V and $89 \pm 13 \mu$ V respectively).

3.2.1.5. Centrality of the superior temporal gyrus (STG). Globally, STG was the less influenced by- and in return had the lowest influence on other structures in the temporal lobe (low ‘total’, ‘in’ and ‘out’ strengths). The superior temporal gyrus was described as the less central node within the temporal lobe.

3.3. Functional modularity in the temporal lobe (Newman's spectral modularity)

Newman's spectral modularity discriminated one module in the amplitude matrix ($p \leq 0.05$, Table 5) showing high mutual amplitude of CCEPs. This module grouped together Amyg, aHipp, pHipp, aPHG and was called Medial (AM-M). The Mann-Whitney-Wilcoxon test showed significant different strengths for AM-M (‘within’: mean = 155 μ V, SE-TW = 30 μ V; ‘between’: mean = 42 μ V, SE-TW = 5 μ V; $p \leq 5 \times 10^{-4}$). The other structures of the network did not show significant modularity but accounted for a segregated complementary Ventro-Latéro-Polar subnetwork (AM-VLP). Mean ‘within’ and ‘between’ strengths in AM-VLP were not significantly different (‘within’: mean = 38 μ V, SE-TW = 3 μ V; ‘between’: mean = 40 μ V, SE-TW = 4 μ V).

4. Discussion

4.1. Interpretation of the probability distribution of averaged amplitudes (AM)

In this study, we analyzed a model of effective connectivity based on the averaged amplitude of CCEPs to characterize the effective organization between medial ‘memory’ and neocortical ‘perceptive’ structures within the temporal lobe. The averaged amplitudes showed a Pareto-like probability distribution with high probability to find low amplitudes and very low probability to find very high averaged amplitudes. All ‘very high’ and ‘high’ amplitudes ($>100 \mu$ V) stemmed from interactions of medial structures with the hippocampus. The hippocampus was the only structure that showed mean amplitude of the O1 peak superior than

200 µV. These amplitudes are in the same range of cognitive evoked potentials recorded in the healthy hippocampus in recognition memory paradigms (Paller and McCarthy, 2002). Properties of the Pareto distribution of averaged O1 peak amplitudes of CCEPs in the temporal lobe could inform us on the functional organization of the network. In this view, neural synchronies (reflected by the amplitude of evoked potentials) could be self-organized critically (Newman, 2005; Kitzbichler et al., 2009; Hesse and Gross, 2014) which is in line with the attractor dynamic of the hippocampus (Wills et al., 2005). The scale-free property of the power law distribution (Newman, 2005) of amplitudes allows the comparison of neural synchronies at different scales. At the behavioral scale, Stevens (1957) showed that ‘prothetic’ stimuli (compared with a standard stimulus) should develop sensations relying on a power law distribution. With both hypotheses that evoked potentials correlate with sensations (MacKay and Fiorentini, 1966), and that amplitudes of evoked potentials could increase with intensity (at least in low range) of the stimulus (Buchsbaum and Silverman, 1968), our results suggest that cognitive tasks inducing a power law distribution of subjective sensations, could rely on strategies involving the medial temporal lobe (Bussey and Saksida, 2007). This observation would be in line with studies suggesting the involvement of the medial temporal lobe during complex perceptive discriminations when the evolving strategy to perform these tasks overloads working memory capacity (Jeneson et al., 2012; Knutson et al., 2012). Such interactions with medial structures could rely on pattern separation hypotheses (Leutgeb et al., 2007; McHugh et al., 2007; Bannerman and Sprengel, 2007) and feed-back modulation of arousal (Davis, 1964).

4.2. Centrality in the temporal lobe: amygdala, anterior hippocampus and rhinal cortex

The anterior hippocampus was central in terms of averaged amplitude of CCEPs. This is in line with the strong ability of synchronization and modulation of large neural populations of the hippocampus within the limbic system described in previous studies (Wilson et al., 1990; Enatsu et al., 2015). The rhinal cortex as well as the amygdala showed lower inward than outward strengths. Low ‘in/out’ amplitude strength could be imputed to the strong asymmetry of reciprocal averaged amplitudes with the anterior hippocampus for the rhinal cortex but not for the amygdala. Low inwards amplitude could be also related to its cytoarchitecture presenting highly integrated nuclei, such as basolateral nuclei, interacting with temporal associative areas (Romanski and LeDoux, 1993; Benarroch, 2015). Thus, the level of synchronization of neural populations within the amygdala could be underestimated due to the non-laminar cytoarchitecture of this structure.

Despite the fact stimulations of the anterior hippocampus evoked highest averaged amplitude of CCEPs in most limbic structures, this structure showed higher inward than outward averaged amplitudes. The rhinal cortex and the amygdala were the only structures that evoked averaged responses at the anterior hippocampus higher than 200 µV. These observations suggest the anterior hippocampus could act as an ‘amplifier’ of afferent information flow from the amygdala or the rhinal cortex as it was observed at the somatic level of pyramidal cells in CA1 region (Andreasen and Lambert, 1999). However, López-Aguado et al. (2001) showed that tissue impedance at the somatic layer of pyramidal cells in CA1 region is significantly higher than in other regions of the hippocampus or the neocortex. They discussed this could lead to biased interpretation of the amplitude of evoked potentials recorded in or generated by the stimulation of the hippocampus. We suggest the high impedance in the CA1 region could represent a functional keystone in the possible ‘amplifying system’ of the hippocampus, analogous to high entry impedance found in the transistor, an elementary electronic device which could serve in

amplifying signal or switching logical information. The anterior hippocampus was found as the shortest path from most of structures in the temporal lobe, towards structures of the limbic system (edges betweenness). In terms of amplitudes, this suggests it could serve in amplifying afferent electrophysiological flows and redistribute this amplification in its targets of the limbic system (recruit larger population of neurons). The hippocampus (CA1) is hypothesized to participate in completion of information (Rolls, 2013) involving distributed areas which were or not primed by sensory inputs. To be reactivated, unprimed multiple-trace memories (Hintzman, 1988) should increase the energy demand which could be provided by the intrinsic and extrinsic amplifying circuit of the anterior hippocampus with limbic structures.

4.3. Non-centrality in the temporal lobe: the superior temporal gyrus

The superior temporal gyrus was the less central node within the temporal lobe. This is in line with previous studies of structural connectivity who showed the superior temporal gyrus shared strong connections with the parietal, frontal, and insular lobes (Rubinov and Sporns, 2011; Lahnakoski et al., 2012) inducing a possible relative lack of effective connectivity within the temporal lobe.

4.4. Functional segregations within the temporal lobe

Newman's spectral modularity extracted one module in the amplitude matrix. The medial temporal lobe (amygdala, hippocampus and rhinal cortex) appeared as the only functional module segregated from neocortical structures and from the posterior parahippocampal gyrus. This suggests a functional dissociation within the temporal lobe between neocortical structures and the medial cortex, which could account for the declarative memory system (Squire and Zola-Morgan, 1991; Canli et al., 2000; Eichenbaum and Cohen, 2001). Also, Wilson et al. (1990) described the posterior parahippocampal gyrus as the most isolated structure from other limbic structures, which could be in line with the separation of the posterior parahippocampal gyrus from medial structures in the present study.

4.5. Limitations and perspectives of this study

Rhinal sulcus, the amygdala, neocortical temporal gyri are morphological landmarks which could handle different cytoarchitectures that are not detectable with anatomical MRI (1.5 T). Therefore, an increased spatial resolution with precise cytoarchitectonic (Keller et al., 2014a; Entz et al., 2014) or thinner sulci-based morphological separation of ROIs (Auzias et al., 2015) could help refining effective organizations of the cerebral cortex, such as the limits between functional modules. Also, the characterization of other features of CCEPs, such as their occurrence and latency (David et al., 2013) could provide different and complementary aspects, such as overlap between modules through features. Averaged amplitude and occurrence have been determined in a large time interval prone to highly variable latencies of CCEPs. The fragmentation of this large temporal window in shorter and consecutive time intervals could provide more precise indices of integration pathways (Keller et al., 2014a). Further signal processing such as generalized eigenvalue decomposition (Hofmanis et al., 2013) or electrode/tissue interface modeling (Trebau et al., 2016) for the separation of the electrical stimulation artifact could enhance the detection of early O1 potentials and could precise characteristics of CCEPs.

Cortico-cortical evoked potentials are routinely applied to epileptic patients as a tool for functional exploration. Because our method has no control population, we may not quantify in what extent some

connectivity patterns have been modulated by the pathological epileptogenicity of a part of the stimulated contacts. In the literature, studies have shown less complex and delayed evoked potentials in the hippocampus sclerosis (Rutecki et al., 1989). Also, enhanced CCEPs have been described in epileptogenic networks compared with sane tissue (Enatsu et al., 2012). This potential bias was minimized by expert visual inspection of all recorded traces and removal of segments with interictal epileptic discharges. The non-correlation of the measure of amplitudes with the diversity of explorations in various pathological cases is in favor of the reproducibility of the model. Also, the correlation of the standard error on amplitudes with amplitudes themselves indicated a high stability of the signal-to-noise ratio through edges, whose mean was high. These characteristics are in favor of a robust and accurate effective connectivity model, but deserves validation in animal models (Dotson et al., 2015; De Curtis et al., 2016) or models with higher number of patients (David et al., 2013; Entz et al., 2014). We cannot exclude that the comparison of a high number of patients separated in different semiological groups could reveal different patterns of effective connectivity within the temporal lobe (Buser et al., 1971; Buser and Bancaud, 1983; Rutecki et al., 1989), which could represent a clinical perspective of our model.

5. Conclusion

We analyzed the effective connectivity within the temporal lobe through the averaged amplitude of the first peak of the CCEP. After

delineating the temporal lobe into eleven ROIs under anatomical landmarks, we applied graph metrics on the effective connectivity matrix and compared functional indices of information transfer through ROIs given the amplitude of the CCEP. The density of probability of averaged amplitudes showed a power law distribution, coherent with a critically self-organized system. In this system, medial temporal structures were central and functionally segregated from the neocortex, generating high mutual CCEP amplitudes. Highest averaged amplitudes of the network, related to interactions with the anterior hippocampus, suggested its role as a signal amplifier of afferent information from amygdala and rhinal cortex with the ability to redistribute this amplification to structures of the limbic system. These observations, from CCEPs, allowed us to discuss current hypothesis of pattern completion achieved by medial structures interacting with the neocortex.

Acknowledgments

The authors wish to thank the anonymous reviewers for useful comments. They also thank Vincent Laprévote, Bruno Rossion, Alain Delconte, David Rudrauf, Olivier David, Patrick Chauvel, Christophe Bernard, Marmaduke Woodman, Jean-Michel Badier, Fabrice Bartolomei, Emmanuel Barbeau, Catherine Liégeois-Chauvel and Hervé Vespignani for useful discussions. The authors are grateful to Valérie Louis-Dorr and Janis Hofmanis for the help in the automatization of analysis.

ANNEX.

Table 2
Patient's Characteristics

Subject number	Age	Sex	Hand	MRI	Epileptogenic zone	Aetiology	Number of electrodes
S1	33	M	R	Negative	Left basal occipito-temporal	Cortical dysplasia	10L-2R
S1bis	33	M	R	Negative	Multifocal: left basal occipito-temporal and left insulo-opercular frontal	Cortical dysplasia	11L
S3	30	F	L	Negative	Left basal temporal (Lateral occipito-temporal sulcus) and medial temporal structures	Cortical dysplasia	8R-6L
S4	41	M	R	Left hippocampal sclerosis	Left medial temporal	Hippocampal sclerosis	13L-1R
S5	33	M	R	Right inferior temporal lesion (Lateral occipito-temporal sulcus dysplasia)	Right basal temporal lobe	Cortical dysplasia	9R-2L
S6	36	F	R	Negative	Left lateral temporal lobe	Cortical dysplasia	11L
S7	37	F	R	Right basal and lateral occipital lesions (DNE)	Infra calcarine of right occipital pole	DNE	9R-1L
S8	30	F	R	Left hippocampal sclerosis/left temporal pole and collateral sulcus atrophies	Left posterior temporal region, angular gyrus	Unknown	12L
S9	34	F	R	Bilateral hippocampal atrophy	Right medial, anterior and posterior temporal structures	Hippocampal sclerosis	8L-5R
S10	46	M	R	Negative	Left anterior temporal lobe and left Insula	Unknown	11L
S11	34	M	R	Left medial temporal dysplasia	Left medial and anterior temporal lobe	Dysplasia	9L-1R
S12	42	F	R	Negative	Left medial temporal structures	Unknown	11L-2R
S13	41	F	R	Bilateral hippocampal sclerosis (mostly left)	Right medial and anterior temporal structures	Hippocampal sclerosis	9R-5L
S14	20	M	R	Left basal temporal and parahippocampal lesions (DNE)	Left basal temporal and parahippocampal DNE	DNE	10L
S15	24	M	R	Hippocampal malformation	Medial temporal structures	Dysplasia	9L-1R
S16	29	F	R	Negative	Left basal temporal and parahippocampal gyrus	Unknown	11L- 3R

Table 3

Number of recorded/stimulated contacts in each ROI and hemisphere through patients. Contacts which have been stimulated twice represent less than five percent of the total number of stimulation runs.

SEEG	Left Hemisphere										Right Hemisphere										TOT.		
	TP	Amyg	aHipp	pHipp	aPHG	pPHG	aFG	pFG	ITG	MTG	STG	TP	Amyg	aHipp	pHipp	aPHG	pPHG	aFG	pFG	ITG	MTG	STG	
S1	–	–	3/1	–	5/1	3/2	4/-	–	8/1	8/3	4/-	–	–	–	–	–	–	–	–	–	–	35/8	
S1bis	–	–	–	–	–	–	–	–	11/7	9/6	6/1	–	–	–	–	–	–	–	–	–	–	26/14	
S3	–	–	4/1	1/1	–	1/-	–	6/5	2/-	6/2	4/-	–	–	5/1	1/1	4/3	4/2	2/2	3/1	2/1	5/1	2/-	52/21
S4	6/1	3/3	3/3	3/2	4/3	–	5/-	6/3	7/-	15/-	9/1	–	–	5/5	–	–	–	–	–	–	2/-	–	68/21
S5	–	3/-	–	–	2/2	–	5/-	–	1/-	4/-	–	–	4/4	4/4	–	6/6	–	3/1	7/4	9/1	26/3	–	74/25
S6	–	4/3	3/2	–	3/3	3/2	3/1	2/2	3/1	12/4	14/2	–	–	–	–	–	–	–	–	–	–	–	47/20
S7	–	–	–	–	–	–	–	–	–	5/-	–	–	–	6/6	–	1/1	–	–	3/2	2/1	14/5	–	31/15
S8	–	–	3/4	–	6/4	–	5/5	9/8	8/6	5/3	6/6	–	–	–	–	–	–	–	–	–	–	–	42/36
S9	7/3	5/2	3/2	–	9/5	–	3/3	–	4/3	6/6	9/4	7/3	4/3	2/1	–	6/5	–	2/2	–	3/1	5/6	–	75/49
S10	9/8	3/1	4/-	–	3/2	–	–	–	5/5	5/5	3/-	–	–	–	–	–	–	–	–	–	–	–	32/21
S11	2/2	4/4	6/3	4/4	4/4	–	3/4	6/5	10/8	6/3	5/2	–	–	4/2	–	–	–	1/1	–	–	2/-	–	57/42
S12	4/4	4/2	4/1	–	2/2	2/2	3/1	2/2	4/2	7/4	8/4	2/-	3/1	4/1	–	–	–	–	–	–	2/-	–	51/26
S13	5/3	2/-	1/1	4/1	1/-	–	–	–	4/1	1/1	7/2	5/3	4/2	–	4/1	3/3	9/5	4/2	9/4	6/4	8/3	–	77/36
S14	7/3	4/2	3/2	3/2	2/2	–	3/2	10/5	3/2	19/5	10/1	–	–	–	–	–	–	–	–	–	–	–	64/26
S15	6/3	3/3	4/4	–	4/3	4/4	–	–	7/4	13/6	2/-	–	–	5/4	–	–	–	–	–	–	5/2	–	53/33
S16	–	–	3/-	2/2	1/1	7/5	4/2	10/6	8/4	15/4	6/2	–	–	2/-	–	6/2	–	5/2	3/-	6/1	–	78/31	
TOT	46/	35/	44/	17/	46/	20/	38/	62/	79/42	136/	81/	16/	39/	3/1	21/	13/7	17/	22/	28/	73/	10/	862/	
27	20	24	12	32	15	18	43	47	23	5	11	26	–	16	–	11	11	8	22	3	424	–	
L + R	62/	51/	83/	20/	67/	33/	55/	84/	107/	209/	91/	–	–	–	–	–	–	–	–	–	–	–	–
	32	31	50	13	48	22	29	54	50	69	26	–	–	–	–	–	–	–	–	–	–	–	–

References

- Almashaikh, T., Rheims, S., Jung, J., Ostrowsky-Coste, K., Montavont, A., De Bellescize, J., Arzimanoglou, A., Keo Kosal, P., Guénod, M., Bertrand, O., Ryvlin, P., 2014a. Functional connectivity of insular efferences. *Hum. Brain Mapp.* 35, 5279–5294.
- Almashaikh, T., Rheims, S., Ostrowsky-Coste, K., Montavont, A., Jung, J., De Bellescize, J., Arzimanoglou, A., Keo Kosal, P., Guénod, M., Bertrand, O., Ryvlin, P., 2014b. Intrainsular functional connectivity in human. *Hum. Brain Mapp.* 35, 2779–2788.
- Andreasen, M., Lambert, J.D.C., 1999. Somatic amplification of distally generated subthreshold EPSPs in rat hippocampal pyramidal neurones. *J. Physiol.* 519 (1), 85–100.
- Auzias, G., Brun, L., Deruelle, C., Coulon, O., 2015. Deep sulcal landmarks: algorithmic and conceptual improvements in the definition and extraction of sulcal pits. *NeuroImage* 111, 12–25.
- Babiloni, C., Bares, M., Vecchio, F., Brazdil, M., Jurak, P., Moretti, D.V., Ubaldi, A., Rossini, P.M., Rektor, I., 2004. Synchronization of gamma oscillations increases functional connectivity of human hippocampus and inferior-middle temporal cortex during repetitive visuomotor events. *Eur. J. Neurosci.* 19 (11), 3088–3098.
- Bancaud, J., Brunet-Bourgoin, F., Chauvel, P., Halgren, E., 1994. Anatomical origin of déjà vu and vivid 'memories' in human temporal lobe epilepsy. *Brain* (117), 71–90.
- Bancaud, J., Talairach, J., 1973. Methodology of stereo EEG exploration and surgical intervention in epilepsy. *Rev. Ot.* 45 (4), 315–328.
- Bannerman, D.M., Sprengel, R., 2007. Remembering the subtle differences. *Science* 317 (5834), 50–51.
- Barbeau, E.J., Taylor, M.J., Regis, J., Marquis, P., Chauvel, P., Liégeois-Chauvel, C., 2008. Spatio temporal dynamic of face recognition. *Cereb. Cortex* 18, 997–1009.
- Barbeau, E., Wendling, F., Regis, J., Duncan, R., Poncet, M., Chauvel, P., Bartolomei, F., 2005. Recollection of vivid memories after perirhinal region stimulations: synchronization in the theta range of spatially distributed brain areas. *Neuropsychologia* 43, 1329–1337.
- Bartolomei, F., Barbeau, E., Gavaret, M., Guye, M., McGonigal, A., Regis, J., Chauvel, P., 2004. Cortical stimulation study of the role of rhinal cortex in déjà vu and reminiscence of memories. *Neurology* (63), 858–864.
- Baxter, M.G., 2009. Involvement of medial temporal lobe structures in memory and perception. *Neuron* (61), 667–677.
- Benarroch, E.E., 2015. The amygdala: functional organization and involvement in neurologic disorders. *Neurology* 84, 1–11.
- Bentin, S., Allison, T., Puce, A., Perez, E., McCarthy, G., 1996. Electrophysiological studies of face perception in humans. *J. Cogn. Neurosci* 8 (6), 551–565. <http://dx.doi.org/10.1162/jocn.1996.8.6.551>.
- Buchsbaum, M.S., Silverman, J., 1968. Stimulus intensity control and the cortical evoked response. *Psychosom. Med.* (30), 12–22.
- Buckley, M.J., Booth, M.C., Rolls, E.T., Gaffan, D., 2001. Selective perceptual impairments after perirhinal cortex ablation. *J. Neurosci.* (21), 9824–9836.
- Bullmore, E., Sporns, O., 2009. Complex brain networks: graph theoretical analysis of structural and functional systems. *Nat. Rev. Neurosci.* 10, 186–198.
- Buser, P., Bancaud, J., Talairach, J., 1971. Electrophysiological studies on the limbic system with multiple multilead stereotaxic electrodes in epileptic patients. In: Proceedings of a symposium held in Paris at Faculté des Sciences, Reprinted from Int. Congress Series n°253. Excerpta Medica, Amsterdam.
- Buser, P., Bancaud, J., 1983. Unilateral connections between amygdala and hippocampus in man. A study of epileptic patients with depth electrodes. *Electroencephal. Clin. Neurophysiol.* 55 (1), 1–12.
- Bussey, T.J., Saksida, L.M., 2007. Memory, perception, and the ventral visual-perirhinal-hippocampal stream: thinking outside of the Boxes. *Hippocampus* (17), 898–908.
- Canli, T., Zhao, Z., Brewer, J., Gabrieli, J.D., Cahill, L., 2000. Event-related activation in the human amygdala associates with later memory for individual emotional experience. *J. Neurosci.* 20 (19), 1–5. RC99.
- Catani, M., Thiebaut de Shotten, M., 2008. A diffusion tensor imaging tractography atlas for virtual in vivo dissections. *Cortex* 44, 1105–1132.
- Catenoix, H., Magnin, M., Guénod, M., Isnard, J., Mauguierre, F., Ryvlin, P., 2005. Hippocampal-orbitofrontal connectivity in human: an electrical stimulation study. *Clin. Neurophysiol.* 116 (8), 1779–1784.
- Catenoix, H., Magnin, M., Mauguierre, F., Ryvlin, P., 2011. Evoked potential study of hippocampal efferent projections in the human brain. *Clin. Neurophysiol.* 122 (12), 2488–2497.
- Chauvel, P., Landré, E., Trottier, S., Vignal, J.P., Biraben, A., Devaux, B., Bancaud, J., 1993. Electrical stimulation with intracerebral electrodes to evoke seizures. *Adv. Neurol.* 63, 115–121.
- Cowell, R.A., Bussey, T.J., Saksida, L.M., 2010. Functional dissociations within the ventral object processing pathway: cognitive modules or a hierarchical continuum? *J. Cogn. Neurosci* 22 (11), 2460–2479.
- Davis, H., 1964. Enhancement of evoked cortical potentials in humans related to a task requiring a decision. *Science* 145 (3628), 182–183.
- David, O., Bastin, J., Chabardès, S., Minotti, L., Kahane, P., 2010. Studying network mechanisms using intracranial stimulation in epileptic patients. *Front. Syst. Neurosci.* 4 (148), 1–10.
- David, O., Job, A.S., De Palma, L., Hoffmann, D., Minotti, L., Kahane, P., 2013. Probabilistic functional tractography of the human cortex. *NeuroImage* 80, 307–317.
- David, O., Woźniak, A., Minotti, L., Kahane, P., 2008. Preictal short-term plasticity induced by intracranial 1Hz stimulation. *NeuroImage* 39, 1633–1646.
- De Curtis, M., Librizzi, L., Uva, L., 2016. The in vitro isolated whole Guinea pig brain as a model to study epileptiform activity patterns. *J. Neurosci. Meth.* 260, 83–90.
- Delorme, A., Makeig, S., 2004. EEGLAB: an open source toolbox for analysis of single-trial EEG dynamics including independent component analysis. *J. Neurosci. Meth.* 134 (1), 9–21.
- Destrieux, C., Fischl, B., Dale, A., Halgren, E., 2010. Automatic parcellation of human cortical gyri and sulci using standard anatomical nomenclature. *NeuroImage* 53 (1), 1–15.
- DeYoe, E.A., Felleman, D.J., Van Essen, D.C., McClendon, E., 1994. Multiple processing streams in occipitotemporal visual cortex. *Nature* 371, 151–154.
- Dotson, N.M., Goodell, B., Salazar, R.F., Hoffman, S.J., Gray, C.M., 2015. Methods, caveats and the future of large-scale microelectrode recordings in the non-human primate. *Front. Syst. Neurosci.* 9 (149), 1–8.
- Duvernoy, H.M., Tamraz, J., Guyot, J., Cabanis, E.A., Iba-Zizen, M.T., Vannson, J.L., 1992. Le cerveau humain: surface, coupes, séries tridimensionnelles et IRM. Springer.
- Eichenbaum, H., Cohen, N.J., 2001. From Conditioning to Conscious Recollection. Oxford University Press, New York.
- Enatsu, R., Gonzalez-Martinez, J., Bulacio, J., Kubota, Y., Mosher, J., Burgess, R.C., Najim, I., Nair, D.R., 2015. Connections of the limbic network: a corticocortical evoked potentials study. *Cortex* 62, 20–33.
- Enatsu, R., Jin, K., Elwan, S., Kubota, Y., Piao, Z., O'Connor, T., Horning, K., Burgess, R.C., Bingaman, W., Nair, D.R., 2012. Correlations between ictal propagation and response to electrical cortical stimulation: a cortico-cortical evoked potential study. *Epilepsy Res.* 101 (1–2), 76–87.
- Entz, L., Tóth, E., Keller, C.J., Bickel, S., Groppe, D.M., Fabó, D., Kozák, L.R., Erőss, L., Ulbert, I., Mehta, A.D., 2014. Evoked effective connectivity of the human neocortex. *Hum. Brain Mapp.* 35 (12), 5736–5753.
- Felleman, D.J., Van Essen, D.C., 1991. Distributed hierarchical processing in the primate cerebral cortex. *Cereb. Cortex* 1 (1), 1–47.
- Friston, K.J., 1994. Functional and effective connectivity in neuroimaging: a synthesis. *Hum. Brain Mapp.* 2, 56–78.
- Girvan, M., Newman, M.E.J., 2002. Community structure in social and biological networks. *Proc. Natl. Acad. Sci.* 99, 7821–7826.
- Grill-Spector, K., 2003. The neural basis of object perception. *Curr. Opin. Neurobiol.* 13, 1–8.
- Halgren, E., Baudena, P., Clarke, J.M., Heit, G., Marinkovic, K., Devaux, B., Vignal, J.P., Biraben, A., 1995. Intracerebral potentials to rare target and distractor auditory and visual stimuli. II. Medial, lateral and posterior temporal lobe. *Electroencephal. Clin. Neurophysiol.* 94, 229–250.
- Halgren, E., Marinkovic, K., Chauvel, P., 1998. Generators of late cognitive potentials in auditory and visual oddball tasks. *Electroencephal. Clin. Neurophysiol.* 106, 156–164.
- He, Y., Evans, A., 2010. Graph theoretical modeling of brain connectivity. *Curr. Opin. Neurotol.* 23, 341–350.
- Hesse, J., Gross, T., 2014. Self-organized criticality as a fundamental property of neural systems. *Front. Syst. Neurosci.* 8 (166), 1–14.
- Hintzman, D.L., 1988. Judgments of frequency and recognition memory in a multiple-trace memory model. *Psychol. Rev.* 95 (4), 528–551.
- Hofmanis, J., Caspary, O., Louis-Dorr, V., Ranta, R., Maillard, L., 2013. Denoising depth EEG signals during DBS using filtering and subspace decomposition. *IEEE Trans. Biomed. Eng.* 60 (10), 2686–2695.
- Huntgeburth, S.C., Petrides, M., 2012. Morphological patterns of the collateral sulcus in the human brain. *Eur. J. Neurosci.* 35, 1295–1311.
- Jeneson, A., Wixted, J.T., Hopkins, R.O., Squire, L.R., 2012. Visual working memory capacity and the medial temporal lobe. *J. Neurosci.* 32 (10), 3584–3589.
- Jonas, J., Frismand, S., Vignal, J.P., Colnat-Coulbois, S., Koessler, L., Vespignani, H., Rossion, B., Maillard, L., 2014. Right hemispheric dominance of visual phenomena evoked by intracerebral stimulation of the human visual cortex. *Hum. Brain Mapp.* 35, 3360–3371.
- Jones, D.K., 2008. Studying connections in the living human brain with diffusion MRI. *Cortex* 44 (8), 936–952.
- Keller, C.J., Bickel, S., Entz, L., Ulbert, I., Milham, M.P., Kelly, C., Mehta, A.D., 2011. Intrinsic functional architecture predicts electrically evoked responses in the human brain. *Proc. Natl. Acad. Sci.* 108 (25), 10308–10313.
- Keller, C.J., Bickel, S., Honey, C.J., Groppe, D.M., Entz, L., Craddock, R.C., Lado, F.A., Kelly, C., Milham, M., Mehta, A.D., 2013. Neurophysiological investigation of spontaneous correlated and anticorrelated fluctuations of the BOLD signal. *J. Neurosci.* 33 (15), 6333–6342.
- Keller, C.J., Honey, C.J., Entz, L., Bickel, S., Groppe, D.M., Toth, E., Ulbert, I., Lado, F.A., Mehta, A.D., 2014a. Cortico-cortical evoked potentials reveal projectors and integrators in human brain networks. *J. Neurosci.* 34 (27), 9152–9163.
- Keller, C.J., Honey, C.J., Mégevand, P., Entz, L., Ulbert, I., Mehta, A.D., 2014b. Mapping human brain networks with cortico-cortical evoked potentials. *Phil. Trans. R. Soc. 369* (1653).
- Kitzbichler, M., Smith, M., Christensen, S., Bullmore, E., 2009. Broadband criticality of human brain network synchronization. *PLoS Comput. Biol.* 5, e1000314. <http://dx.doi.org/10.1371/journal.pcbi.1000314>.
- Knutson, A.R., Hopkins, R.O., Squire, L.R., 2012. Visual discrimination performance, memory, and medial temporal lobe function. *Proc. Natl. Acad. Sci.* 109 (32), 13106–13111.
- Kravitz, D.J., Kadharbatcha, S.S., Baker, C.I., Ungerleider, L.G., Mishkin, M., 2013. The ventral visual pathway: an expanded neural framework for the processing of object quality. *Trends Cogn. Sci.* 17 (1), 26–49.
- Lacruz, M.E., García Seoane, J.J., Valentín, A., Selway, R., Alarcón, G., 2007. Frontal and temporal functional connections of the living human brain. *Eur. J. Neurosci.* 26, 1357–1370.
- Lahnakoski, J.M., Gleean, E., Salmi, J., Jääskeläinen, I.P., Sams, M., Hari, R., Nummenmaa, L., 2012. Naturalistic fMRI mapping reveals superior temporal sulcus

- as the hub for the distributed brain network for social perception. *Front. Hum. Neurosci.* 6 (223).
- Leutgeb, J.K., Leutgeb, S., Moser, M.B., Moser, E.I., 2007. Pattern separation in the dentate gyrus and CA3 of the hippocampus. *Science* 315, 961–966.
- Liégeois-Chauvel, C., Bénar, C., Krieg, J., Delbé, C., Chauvel, P., Giusiano, B., Bigand, E., 2014. How functional coupling between the auditory cortex and the amygdala induces musical emotion: a single case study. *Cortex* 60, 82–93.
- López-Aguado, L., Ibarz, J.M., Herreras, O., 2001. Activity-dependent changes of tissue resistivity in the CA1 region *in vivo* are layer-specific: modulation of evoked potentials. *Neuroscience* 108 (2), 249–262.
- MacKay, D.M., Fiorentini, A., 1966. Evoked potentials correlated with a visual anomaly. *Nature* 209 (5025), 787–789.
- Maris, E., Oostenveld, R., 2007. Nonparametric statistical test of EEG- and MEG-data. *J. Neurosci. Meth.* 164, 177–190.
- Matsumoto, R., Nair, D.R., LaPresto, E., Mikuni, N., Najm, I., Bingaman, W., Shibasaki, H., Lüders, H.O., 2004. Functional connectivity in the language system: a cortico-cortical evoked potential study. *Brain* 127, 2316–2330.
- Matsumoto, R., Nair, D.R., LaPresto, E., Mikuni, N., Najm, I., Bingaman, W., Shibasaki, H., Lüders, H.O., 2007. Functional connectivity in human cortical motor system: a cortico-cortical evoked potential study. *Brain* 130, 181–197.
- McHugh, T., Jones, M.W., Quinn, J.J., Balthasar, N., Coppari, R., Elmquist, J.K., Lowell, B.B., Fanselow, M.S., Wilson, M.A., Tonegawa, S., 2007. Dentate gyrus NMDA receptors mediate rapid pattern separation in the hippocampal network. *Science* 317, 94–99.
- Mishkin, M., Ungerleider, L., 1982. Contribution of striate inputs to the visuospatial functions of parieto-preoccipital cortex in monkeys. *Behav. Brain Res.* 6, 57–77.
- Moss, H.E., Rodd, J.M., Stamatakis, E.A., Bright, P., Tyler, L.K., 2005. Anteromedial temporal cortex supports fine-grained differentiation among objects. *Cereb. Cortex* 15, 616–627.
- Newman, M.E.J., 2005. Power laws, pareto distributions and zipf's law. *Contemp. Phys.* 46 (5), 323–351.
- Newman, M.E.J., 2006. Modularity and community structure in networks. *Proc. Natl. Acad. Sci.* 103 (23), 8577–8582.
- Paller, K.A., McCarthy, G., 2002. Field potentials in the human hippocampus during the encoding and recognition of visual stimuli. *Hippocampus* 12, 415–420.
- Rey, H.G., Fried, I., Quiroga, R., 2014. Timing of single-neuron and local field potential responses in the human medial temporal lobe. *Curr. Biol.* 24, 299–304.
- Rolls, E.T., 2013. The mechanisms for pattern completion and pattern separation in the hippocampus. *Front. Syst. Neurosci.* 7 (74), 1–21. <http://dx.doi.org/10.3389/fnsys.2013.00074>.
- Romanski, L.M., LeDoux, J.E., 1993. Information cascade from primary auditory cortex to the amygdala: corticocortical and corticoamygdaloid projections of temporal cortex in the rat. *Cereb. Cortex* 3 (6), 516–532.
- Rossoni, B., Caldera, R., Seghier, M., Schuller, A.M., Lazeyras, F., Mayer, E., 2003. A network of occipito-temporal face-sensitive areas besides the right middle fusiform gyrus is necessary for normal face processing. *Brain* 126 (11), 2381–2395.
- Rubinov, M., Sporns, O., 2010. Complex network measures of brain connectivity: uses and interpretations. *NeuroImage* 52, 1059–1069.
- Rubinov, M., Sporns, O., 2011. Weight-conserving characterization of complex functional brain networks. *NeuroImage* 56, 2068–2079.
- Rutecki, P.A., Grossman, R.G., Armstrong, D., Irish-Lowen, S., 1989. Electro-physiological connections between the hippocampus and entorhinal cortex in patients with complex partial seizures. *J. Neurosurg.* 70, 667–675.
- Squire, L.R., Zola-Morgan, S., 1991. The medial temporal lobe memory system. *Science* 253, 1380–1386.
- Stevens, S.S., 1957. On the psychophysical law. *Psychol. Rev.* 64, 153–181.
- Suzuki, W.A., 2009. Perception and the medial temporal lobe: evaluating the current evidence. *Neuron* 61, 657–666.
- Tadel, F., Baillet, S., Mosher, J.C., Pantazis, D., Leahy, R.M., 2011. Brainstorm: a user-friendly application for MEG/EEG analysis. *Comput. Intell. Neurosci.*, 879716.
- Tanaka, K., 1996. Inferotemporal cortex and object vision. *Annu. Rev. Neurosci.* 19, 109–139.
- Trebaul, L., Rudrauf, D., Job, A.S., Mâlia, M.D., Popa, I., Barborica, A., Minotti, L., Mîndruță, I., Kahane, P., David, O., 2016. Stimulation artifact correction method for estimation of early cortico-cortical evoked potentials. *J. Neurosci. Meth.* 264, 94–102.
- Valentín, A., Anderson, M., Alarcón, G., García Seoane, J.J., Selway, R.P., Binnie, C.D., Polkey, C.E., 2002. Responses to single pulse electrical stimulation identify epileptogenesis in the human brain *in vivo*. *Brain* 125, 1709–1718.
- Van den Heuvel, M.P., Sporns, O., 2011. Rich-club organization of the human connectome. *J. Neurosci.* 31 (44), 15775–15786.
- Wang, J.H., Zuo, X.N., Gohel, S., Milham, M.P., Biswal, B.B., He, Y., 2011. Graph theoretical analysis of functional brain networks: test-retest evaluation on short- and long-term resting-state functional MRI data. *PLoS One* 6 (7), e21976. <http://dx.doi.org/10.1371/journal.pone.0021976>.
- Warren, D.E., Duff, M.C., Jensen, U., Tranel, D., Cohen, N.J., 2012. Hiding in plain view: lesions of the medial temporal lobe impair on-line representation. *Hippocampus* 22 (7), 1577–1588.
- Wills, T.J., Lever, C., Cacucci, F., Burgess, N., O'Keefe, J., 2005. Attractor dynamics in the hippocampal representation of the local environment. *Science* 308 (5723), 873–876.
- Wilson, C.L., Isokawa, M., Babb, T.L., Crandall, P.H., 1990. Functional connections in the human temporal lobe. I. Analysis of limbic system pathways using neuronal responses evoked by electrical stimulation. *Exp. Brain Res.* 82, 279–292.
- Wilson, C.L., Isokawa, M., Babb, T.L., Crandall, P.H., Levesque, M.F., Engel, J., 1991. Functional connections in the human temporal lobe. II. Evidence for a loss of functional linkage between contralateral limbic structures. *Exp. Brain Res.* 85, 174–187.
- Zeki, S., Shipp, S., 1988. The functional logic of cortical connections. *Nature* 335, 311–317.